Computers and Chemical Engineering xxx (2016) xxx–xxx

Contents lists available at ScienceDirect

Computers and Chemical Engineering

journal homepage: www.elsevier.com/locate/compchemeng

Particle filter based hybrid prognostics of proton exchange membrane fuel cell in bond graph framework

Mayank Shekhar Jha[a,*], Mathieu Bressel[b,c], Belkacem Ould-Bouamama[b], Genevieve Dauphin-Tanguy[a]

[a] CRIStAL UMR CNRS 9189, Ecole Centrale de Lille, Cité Scientifique, 59650, Villeneuve d'Ascq, France
[b] CRIStAL UMR CNRS 9189, Polytech Lille, Université de Lille 1, Cité Scientifique 59650 Villeneuve d'Ascq, France
[c] FEMTO-ST, UMR CNRS 6174, FCLAB, FR CNRS 3539, Rue Thierry Mieg, 90000 Belfort, France

ARTICLE INFO

Article history:
Received 16 June 2016
Received in revised form 6 August 2016
Accepted 11 August 2016
Available online xxx

Keywords:
Prognostics
Bond graph
Particle filters
PEM fuel cell
Remaining useful life

ABSTRACT

This paper presents a holistic solution towards prognostics of industrial Proton Exchange Membrane Fuel Cell. It involves an efficient multi-energetic model suited for diagnostics and prognostics, developed using some specific properties of Bond Graph (BG) theory. The benefits of Particle Filters (PF) are integrated with the BG model derived fault indicators named Analytical Redundancy Relations, for prognostics of the Electrical-Electrochemical part. The hybrid prognostics involves statistical degradation model obtained using real degradation tests. Prognostics problem is formulated as the joint state-parameter estimation problem in PF framework where estimations of state of health (SOH) is obtained in probabilistic domain. This in turn is used for prediction of Remaining Useful Life (RUL) under constant current as well as dynamic current solicitations. The SOH estimation and RUL prediction is obtained with very high accuracy and precise confidence bounds. Moreover, a comparative analysis with Extended Kalman Filter demonstrates the usefulness of PF.

1. Introduction

Addressing the issue of sustainable energy requirement has become a major challenge, especially as the world faces major decline of the available fossil energy resources and global warming. Usage of hydrogen as the energy source and development of Proton Exchange Membrane Fuel Cell (PEMFC) has emerged as one of the promising solutions and a potential alternative to the fossil energy (Ziogou et al., 2011). However, several factors inhibit the wide utility of PEMFC such as irreversible degradation mechanisms, multiple impairments etc. These manifest in form of deterioration of the carbon support, the dehydration of the membrane, a catalytic degradation and the ripening of the platinum particles (Martínez et al., 2008; Schmittinger and Vahidi, 2008). These phenomena generate voltage drops which are difficult to forecast when a constant or variable profile of load (current) is considered (Pei and Chen, 2014). Most of the phenomena described above are mutually dependent and understood with insufficient clarity. The presence of irreversible degradation severely affects the useful life of PEMFC and leads to inefficiency, reduced lifespan, lesser power density and high maintenance cost (Venkatasubramanian, 2005). This in turn reduces the reliable deployment of PEMFC, thus preventing its widespread use. The latter has led to an urgent need of effective pro-active maintenance strategies against the traditional preventive action ones. The latter lead to enhancement in the useful life of PEMFC and reduction in the maintenance cost. The issue of useful life assessment is best addressed from the perspectives of Prognostic and Health Management (PHM) (Dai et al., 2013; Jardine et al., 2006). For instance, knowledge of the Remaining Useful Life (RUL) of a fleet of energy sources (e.g. batteries (Hu et al., 2014; Ng et al., 2014) and PEMFC (Chen et al., 2015)) leads to good estimation of the power that can be delivered to adapt the energy distribution. This enhances the service time of the system and economic investment.

Thus, the core problem at hand can be seen in two folds: complex and mutually dependent multi-energetic physics of PEMFC along

Abbreviations: ARR, analytical redundancy relations; BG, bond graph; BG-LFT, bond graph in linear fractional transformation; DM, degradation model; DPP, degradation progression parameter; EE, electrical-electrochemical; EKF, extended kalman filter; EOL, end of life; ESCA, electro-chemical active surface area; FC1, fuel cell under constant current load; FC2, fuel cell under variable current load; GDL, gas diffusion layer; I-ARR, interval valued analytical redundancy relations; OCV, open circuit voltage; PDF, probability density function; PEMFC, proton exchange membrane fuel cell; PF, particle filters; PHM, prognostic and health management; *RA*, relative accuracy; RMAD, relative median absolute deviation; *RMSE*, root mean square error; RUL, remaining useful life; SIR, sampling importance resampling; SOH, state of health.

* Corresponding author.
E-mail addresses: jha.mayank.jha@gmail.com, jha@insa-toulouse.fr (M.S. Jha).

http://dx.doi.org/10.1016/j.compchemeng.2016.08.018

Notations

I_0	Exchanged current in PEMFC
I_{fc}	Load Current in PEMFC
I_L	Limiting Current in PEMFC
$Rohm$	Global Resistance
n_s	Number of cells in a stack
U_{fc}	Stack Voltage sensor
θ^d	System parameter under degradation
θ_n^d	Nominal value of θ^d
$\Delta\theta$	Additive uncertainty on θ
δ_θ	Multiplicative uncertainty on θ
$r_n(t)$	Numerical evaluation of the nominal part of ARR
y_k^d	Measurement of prognostic candidate $\theta^d(or, \alpha)$ at discrete time k
γ^d	Degradation progression parameter associated to θ^d
$\hat{X}$	Estimated value of species X
X^*	True value of species X
σ_X	Standard deviation value of random specie X
σ_X^2	Variance of population values of X
N	Number of particles in PF
w_k^i	Weight of i^{th} particle at discrete time k
$w^d(t)$	Noise associated with the measurements y_k^d
α	Bounds of true RUL in $\alpha - \lambda$ metric for RUL assessment
α	State of health indicator
β	Rate of change of α
ξ_k	Normally distributed artificial random-walk noise

with the irreversible degradation mechanisms involved, and the requirement of efficient assessment of the RUL for development of efficient pro-active maintenance strategies.

Recently, Jha et al. (2016) proposed a hybrid prognostics methodology where benefits of Bond graph (BG) modelling technique and Sequential Monte Carlo based *Particle filters* (PF) were integrated for efficient prognostics. As such, statistical or empirical *degradation models* (DM) could be exploited along with information obtained from physics based models.

This paper implements the methodology proposed in Jha et al. (2016) in the context of PEMFC. As such, a holistic solution is developed towards aforementioned issues related to PEMFC. The first issue is tackled in BG framework where mutually-dependent complex dynamics of PEMFC is systematically modeled and graphically represented. The second issue of prognostics is addressed for the electrical-electrochemical (EE) part of PEMFC in PF framework. To that end, the electrical global resistance parameter is considered uncertain. Also, based upon the aging tests conducted in real time, the global resistance and limiting current are considered as the principle system-parameters undergoing significant degradation. To achieve a robust detection of degradation beginning, uncertain BG model named BG in Linear Fractional Transformation (BG-LFT) (Sié Kam and Dauphin-Tanguy, 2005), is developed for the EE part. This enables a robust detection of degradation-beginning in form of an incipient parametric fault. Thereafter, prognostics is exercised using PFs.

To this end, a *fault model* is constructed in state space modelling the dynamics of state of health (SOH) evolution. The latter is inspired from the DM and observation equation is obtained from the uncertain BG derived fault indicators or Analytical Redundancy Relations (ARRs). This way, the ARR used as the degradation indicator, is further exploited to obtain SOH evolution information. Using PF algorithms, SOH estimation is obtained along with the estimation of the associated unknown parameter that influences the degradation evolution. The latter is tracked to obtain the SOH in probabilistic terms. These estimations are projected in future, to achieve RUL predictions of the EE part of PEMFC. The methodology is applied on real degradation data sets under constant and dynamic load (current) profiles.

Various motivations for the development of this work are:

- There are very few existing model-based works that propose efficient prognostics for PEMFC. Wang et al. (2011) proposes physics based DM of the Electro-Chemical Active Surface Area (ECSA), used for damage tracking and prediction using Unscented Kalman Filter. However, ECSA is only one of the many factors that influence the damage progression. As such, more efficient approaches are needed. (Chen et al., 2015) proposed a rapid lifetime prediction formula to estimate the voltage drop rate. However, with only a linear DM employed, it required further investigation.
- Recently, (Jouin et al., 2014a,b, 2015) have efficiently exploited PFs for efficient prognostics of PEMFC. Therein, DM considered is purely empirical in nature, employing a model fitting log-linear DM. As such, it lacks the insight into the physics of the phenomenon. On the contrary, in this work, based on aging tests, SOH is considered to evolve linearly. Moreover, although the DM is statistically derived, the measurement of degradation state is obtained from the ARR which reflects the energetic assessment of EE part. As such, understanding of the underlying physics is not compromised during the process of prognostics.
- Contrary to constant current solicitations, dynamic solicitations are more representative of the current load profiles encountered in practice (residential applications under changing weather-temperature conditions (Oh et al., 2012)). The latter have not been studied much (Bressel et al., 2016b). In fact, presence of variable speed of degradation progression, reduces the effectiveness of model based approaches for prognostics. Moreover, machine learning techniques remain useful to a limited extent as they require many examples/samples of similar degradation patter. In this context, this paper shows that PFs are able to estimate the damage pattern efficiently and generate precise RUL predictions.
- Interestingly, the issue of PEMFC prognostics based in BG framework has not even been attempted. For instance, although Saisset et al. (2006) and Peraza et al. (2008) develop a detailed PEMFC BG model, they are not suited for diagnostics or prognostics. Ould-Bouamama et al. (2013) develops Signed BG model of PEMFC, but for diagnostics purposes only.

The scientific interests and novel contributions of this paper are listed as follows.

- BG model of industrially oriented PEMFC is developed with efficient functional decomposition suited for diagnostics and prognostics.
- An efficient robust detection of parametric-degradation-beginning is achieved by development of BG-LFT model of the electrical-electrochemical part.
- Benefits of BG modelling technique and Monte Carlo framework are integrated for estimation of SOH and RUL prediction in PEMFC context.
- The method is applied on EE part of PEMFC under: (i) constant current load stack solicitation, (ii) Dynamic (variable) current load solicitations, using real/experimental degradation data sets.
- The SOH estimator is replaced with Extended Kalman Filter (EKF) for constant current load case and the performance is compared with that of PF.

Besides this introduction section, Section 2 discusses the background and related works, Section 3 details the BG model of the PEMFC, Section 4 builds the BG-LFT model of the EE part and

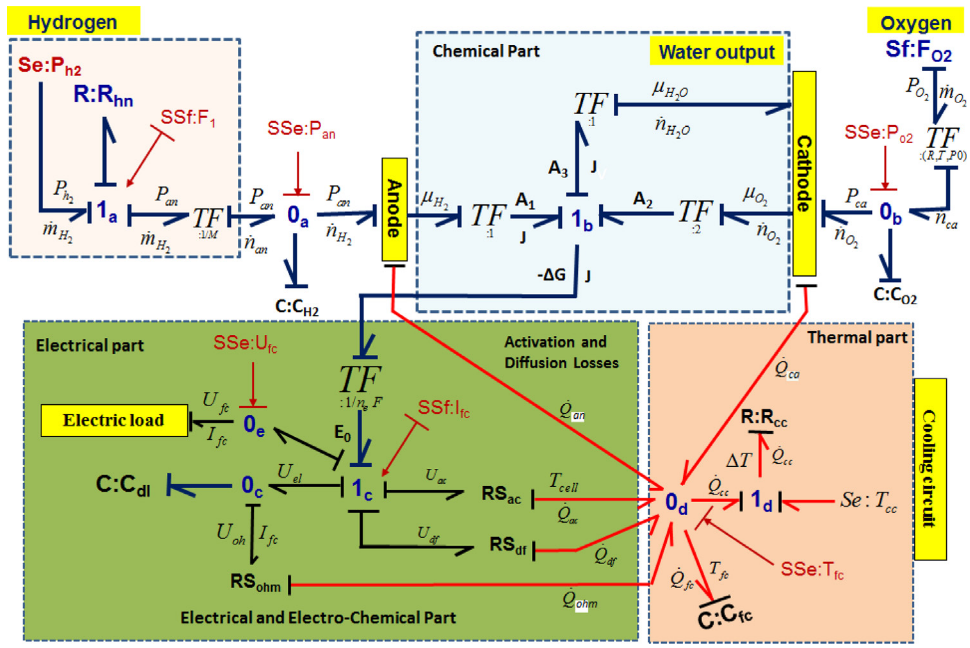

Fig. 1. Bond graph model of the PEMFC in preferred derivative causality.

describes the ARR derivation and adaptive thresholds. Section 5 details the degradation tests in real time and Section 6 discusses the methodology of prognostics. Then, Section 7 provides the various evaluation metrics. Section 8 details the results and associated discussions. Finally, conclusions are drawn in Section 9.

2. Background and related works

2.1. Bond graph related works

BG has been extensively used owing to the behavioral, structural and causal properties (Mukherjee and Samantaray, 2006), that provide a systematic approach towards development of supervision and fault detection and Isolation (FDI) of highly non-linear and complex thermo-chemical systems (Ould-Bouamama et al., 2012), complex hydraulic systems (Zhang and Hoo, 2011) etc. In BG framework, the model based FDI is mainly based upon ARRs (Bouamama et al., 2003; Jha et al., 2014; Samantaray and Bouamama, 2008). For deterministic systems, the properties and ARR generation algorithm are well detailed in Bouamama et al. (2003). Moreover, BG-LFT has been widely implemented for robust diagnosis (to avoid false alarms) through generation of adaptive thresholds with respect to parametric uncertainties (Djeziri et al., 2011, 2007, 2009; Jha et al., 2014).

2.2. Hybrid prognostics and particle filter based works

Hybrid prognostics approaches (Sikorska et al., 2011; Vachtsevanos et al., 2007) combine the advantages of the model based approaches (Jardine et al., 2006) and data-driven prognostics (Schwabacher, 2005), in that they employ physics or statistical based DMs, and use the measured information to adapt the estimation of damage progression. Thus, the un-modeled variations and environmental changes, external noise etc. are efficiently managed for estimation of state of health state and subsequent RUL predictions.

Based in Monte-Carlo framework, PF or Sequential Monte Carlo methods (Arulampalam et al., 2002), have been extensively exploited for prognostic purposes. Most of the previous attempts involving PFs provide the RUL predictions based upon the estimate of the current state of health of the system parameter (concerned prognostics candidate) and state of the hidden parameters that influence the damage-progression/degradation. The issue of current health estimation is usually addressed as joint state-parameter estimation problem (Daigle and Goebel, 2011). Then, the RUL predictions are obtained as probability distributions that take into account various inherent uncertainties (Daigle and Goebel, 2011, 2013). Significant works include prediction RUL prediction of PEMFC (Jouin et al., 2014a,b, 2015), assessment of RUL in lithium-ion batteries (Saha and Goebel, 2009), battery health monitoring (Saha et al., 2009a), prediction of crack growth (Zio and Peloni, 2011), application to pneumatic valve (Daigle and Goebel, 2011), prediction of wear (Daigle and Goebel, 2013) etc. Comprehensive studies on various optimal or sub-optimal filters for prognostic purposes are found in An et al. (2015), Daigle et al. (2012), Saha et al. (2009a,b).

3. Bond graph model of PEMFC

PEMFC is an electrochemical converter which converts the chemical energy of hydrogen and oxygen into DC electricity that flows in an external electrical load. It is based on the reverse principle of electrolysis. The well-established basic chemistry of PEMFC is omitted in this paper. The latter can be found detailed in Larminie et al. (2003). Instead, the physics based-BG model built to achieve the objectives of this paper is presented in Fig. 1. The global PEMFC system is decomposed into various subsystems. The inputs and outputs for each of the subsystems are the exchanged-powers represented by two conjugated power variables: effort and flow (graphically shown by a half-arrow). Depending on the physical field considered, the power variables have their respective meaning. For instance, the electrical system involves the pair voltage-current (U, i), thermal convection involves the pair temperature-enthalpy flow $(T, \dot{H})$, thermal conduction involves the pair temperature-thermal flow $(T, \dot{Q})$, pressure-mass flow $(P, \dot{m})$ models the hydraulic phenomenon, the pair affinity-speed of reaction (A, J) models the chemical and electrochemical transformation phenomenon and the pair chemical potential-molar flow $(\mu, \dot{n})$ for chemical reaction. As the initial conditions are not fully known

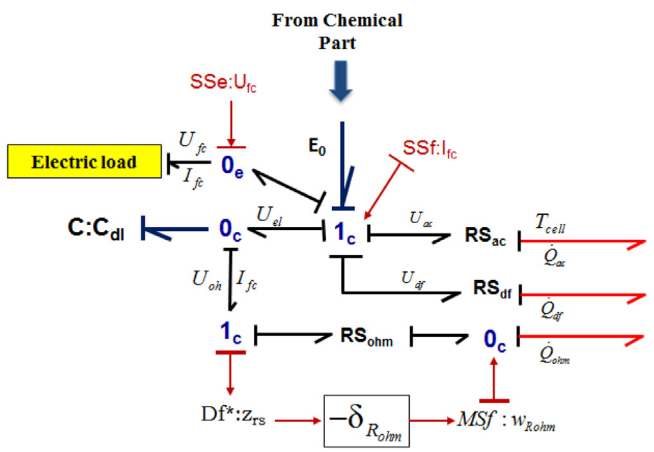

Fig. 2. BG-LFT model of Electrical-Electrochemical subsystem.

in a real process, the derivative causality (suited for diagnostics (Bouamama et al., 2003)) is preferred to the integral causality (close to the reality of physics, suited for simulation purposes (Mukherjee and Samantaray, 2006)). Employment of derivative causality avoids unknown initial condition problem for ARR generation process. Moreover, all the detectors (*De* for the effort detector and *Df* for the flow detector) are dualized into *sources of signal SSe* and *SSf* respectively. The latter are used as inlet nodes in the unknown variable elimination oriented graph (Samantaray and Bouamama, 2008).

3.1. Hydrogen inlet and oxygen inlet

As shown in Fig. 1, source of hydrogen is represented by Se : P_{H_2} where the corresponding pressure P_{H_2} is a known quantity. The valve represented by a resistive BG element $R : Rh_n$ (where subscript n denotes the nominal value) regulates the flow of hydrogen (measured by $SSf : F_{H2}$). The pressure on the anode compartment is measured by the pressure sensor $SSe : P_{an}$. The hydraulic dynamics (storage of gases) is represented with the capacitive elements $C : C_{H2}$ for anode. To transform the mass flow (kg/s) into a molar flow (mole/s), a transformer element $\underset{:1/M}{TF}$ is used where M is the modulus representing the molar mass (kg/mol). Flow sensor $SSf : F_{H2}$ measures the mass flow rate $\dot{m}_{H_2}$. Non-linear Bernoulli equation links the pressure across the valve P_{Rh}, and the flow $\dot{m}_{H_2}$ through the valve, as:

$$P_{Rh} = R_{hn}(\dot{m}_{H2})^2 \tag{1}$$

3.2. Oxygen inlet

In the similar fashion, $Sf : F_{O2}$ represents the source of oxygen inlet flow, pressure sensor $SSe : P_{O2}$ measures the pressure on the anode compartment, the hydraulic dynamics (storage of gases) is represented by the capacitive BG elements $C : C_{O2}$ for cathode, a transformer element $\underset{:(R,T,P0)}{TF}$ transforms the mass flow(kg/s) into a molar flow (mole/s).

3.3. Chemical part

The reduction-oxidation reaction (driven by the chemical affinity) is modeled using the Gibbs free energy ΔG in the 1_b junction as,

$$\Delta G = A_1 + A_2 - A_3 \tag{2}$$

$$A_1 = \mu_{H2}, \quad A_2 = \frac{1}{2}\mu_{O2}, \quad A_3 = \mu_{H2O} \tag{3}$$

$$\mu_{H2} = \mu_0^{H2} + RT_{H2}\ln(P_{H2}) \tag{4}$$

$$\mu_{O2} = \mu_0^{O2} + RT_{O2}\ln(P_{O2}) \tag{5}$$

$$\mu_{H2O} = \mu_0^{H2O} \tag{6}$$

where R is the perfect gas constant,μ_x is the chemical potential of species x and the water is in liquid phase. The three transformer elements therein,$\underset{:\nu_i}{TF}(i = 1, 2, 3)$, have their respective modulus ν_i, that represent the stoichiometric coefficients of the reactants ($\nu_1 = 1$ for hydrogen and $\nu_2 = 2$ for oxygen) and the product water with $\nu_3 = 1$.

3.4. Electrical and electro-Chemical (EE) part

The EE subsystem accounts for electrical part and activation-diffusion losses. The kinetics of reaction as shown in (2), generates an over-voltage which is termed as activation loss. Furthermore, the resistivity of the membrane electrode assembly decreases the operational potential due to the Ohmic effect. The resistance value depends on the degree of humidification of the membrane and on the temperature. Finally, the reactive species are consumed and imply a loss of partial pressure on the reaction surfaces. The latter phenomenon significantly reduces the Nernst potential, especially at high currents (Larminie et al., 2003). This phenomenon is called diffusion/concentration losses (Park et al., 2015). Moreover, during transients, electron accumulation along the membrane electrode interface is observable. It is the double layer capacitance effect.

In the BG model, the EE subsystem and the chemical part are connected using the transformer $\underset{:1/n_e\ F}{TF}$. This results in obtaining the thermodynamic potential E_0 as,

$$E_0 = -\frac{\Delta G}{n_e F} = -\frac{A_1 + A_2 - A_3}{n_e F} \tag{7}$$

where n_e is the number of electron involved in the reaction and F is the number of Faraday. RS is an active two port dissipative (resistive) element that generates thermal energy. The two port thermal dissipative element RS_{ohm} models the Ohmic losses (membrane, electrodes and connectors). Similarly, the activation and the diffusion phenomenon are modeled by RS_{ac} and RS_{df} respectively. The associated power variables are related as,

$$U_{ac} = ATln\left(\frac{I_{fc}}{I_0}\right) \tag{8}$$

$$U_{df} = BTln\left(1 - \frac{I_{fc}}{I_L}\right) \tag{9}$$

where, A is the activation constant;$A = R/\chi nF$ and B is the diffusion constant; $B = -RT/\chi nF$ with χ as the transfer coefficient,I_0 is the exchanged current, I_{fc} is the load current and I_L is the limiting current i.e. maximal current the fuel cell is able to provide. The double layer capacitance phenomenon is modeled by a capacitor element $C : C_{dl}$ and imposes the dynamics of the activation phenomenon. *Uel* is expressed at the junction $\mathbf{0}_C$, as the solution of the equation:

$$I_{fc} = \frac{Uel}{Rohm} + Cdl\frac{dUel}{dt} \tag{10}$$

where *Rohm* is the global resistance (membrane and connectors).

3.5. Thermal part

The active elements and the chemical reaction being exothermic, generate heat that needs to be evacuated by means of a cooling system. The thermal resistance of the PEMFC and cooling circuit is modeled by the passive resistive element $R : R_{cc}$ (representing the thermal resistance). The thermal dynamics is fixed by the thermal capacitance $C : C_{fc}$ which depends on the fuel cell temperature (measured by the temperature sensor SSe: T_{fc}) and the ambient temperature is represented by an effort source Se: T_{cc}. The various power variables are related as,

$$\dot{Q}_{ca} = \Delta S_{H2O}\,\dot{n}_{H2O} - \Delta S_{O2}\;\dot{n}_{O2} \tag{11}$$

$$\dot{Q}_{an} = -\Delta S_{H2}\;\dot{n}_{H2} \tag{12}$$

$$\dot{Q}_{ohm} = \frac{U_{fc}^2}{R_{ohm}} \tag{13}$$

$$\dot{Q}_{fc} = C\frac{dT_{cc}}{dt} \tag{14}$$

$$\dot{Q}_{cc} = R_{cc}\left(T_{fc} - T_{cc}\right) \tag{15}$$

$$\dot{Q}_{df} = R_{df} I_{fc}^2 \tag{16}$$

$$\dot{Q}_{ac} = R_{ac} I_{fc}^2 \tag{17}$$

where $\dot{n}_x$ is the molar flow and $\Delta S_x = \Delta S_{x_0} + \int_{298}^{T} \frac{Cp}{\theta} d\theta$ is the flow of entropy of the specie x.

4. Generation of determinist ARRs and robust thresholds

In this work, the determinist ARRs are derived through energetic assessment at the junctions of BG model in preferred derivative causality of Fig. 1. The BG-LFT model of EE subsystem can be used to derive uncertain ARRs in presence of additive or multiplicative uncertainties. An uncertain ARR can be decoupled into nominal and uncertain parts (Djeziri et al., 2011, 2007, 2009).

4.1. Derivation of determinist ARRs of PMFC

In BG context, ARR is a constraint expression being a function of system parameters and known variables as,

$$ARR : f(SSe, SSf, Se, Sf, MSe, MSf, \boldsymbol{\theta}) \tag{18}$$

where $\boldsymbol{\theta}$ is vector of system parameters. The numerical evaluation of the ARR gives a residual r, $r = Eval[ARR]$. For detailed description of ARR derivation method and application of the latter, readers are referred to Bouamama et al. (2003), Djeziri et al. (2007), and Ould-Bouamama et al. (2012). In Fig. 1, at junction $\mathbf{1}_a$ (associated with flow sensor SSf: F_{H2}), the ARR candidate is deduced using power conservation law: sum of efforts is equal to zero,

$$ARR_1 : P_{H_2} - P_{an} - P_{Rh} = 0 \tag{19}$$

Based on covering causal paths, using (1) and known variables, $P_{H2} = Se : P_{H2}$, $P_{an} = SSe : P_{an}$ and $\dot{m}_{H_2} = SSf : F_{H2}$, (14) is expressed as,

$$ARR_1 = SSe : P_{H_2} - SSe : P_{an} + R_{hn}(F_{H2})^2 \tag{20}$$

This ARR can be used to monitor the flooding (such as valve blockage) in the channels of the PMFC. The latter does not form the interest of this paper. The second ARR is deduced from junction $\mathbf{1}_c$:

$$ARR_2 : n_s\left(E_0 - U_{ac} - U_{df} - U_{el}\right) - U_{fc} = 0 \tag{21}$$

where n_s is number of cells in a stack. Here, $n_s = 1$. From (4)–(9) and (10), the unknown variables can be eliminated using causal paths and known electro-chemical relations, such that ARR_2 is expressed as:

$$ARR_2 = n_s\left(\begin{array}{c}\mu_0^{H2} + RT_{H2}\ln(P_{H2}) + \frac{1}{2}\left[\mu_0^{O2} + RT_{O2}\ln(P_{O2})\right] - \mu_0^{H2O} \\ - R_{ohm}I_{fc} - ATln\left(\frac{I_{fc}}{I_0}\right) - BTln\left(1 - \frac{I_{fc}}{I_l}\right)\end{array}\right) - SSe : U_{fc} \tag{22}$$

Note that due to fast electrical dynamics (10) has been approximated as (De Bruijn et al., 2008),

$$Uel = R_{ohm}.I_{fc} \tag{23}$$

ARR_2 is sensitive to drying, flooding and aging of the fuel cell. The latter form the main focus of this paper. The third ARR is derived from junction $\mathbf{0}_d$ in the thermal field:

$$ARR_3 : \dot{Q}_{ac} + \dot{Q}_{df} + \dot{Q}_{an} + \dot{Q}_{ca} + \dot{Q}_{ohm} - \dot{Q}_{cc} - \dot{Q}_{fc} = 0 \tag{24}$$

From(6)-(12), the unknown variables are eliminated to express (24) as,

$$ARR_3 = R_{ac}I_{fc}^2 + R_{df}I_{fc}^2 - R_{cc}\left(T_{fc} - T_{cc}\right) - C\frac{dT_{cc}}{dt} + \frac{U_{fc}^2}{R_{ohm}} - \Delta S_{H2}\dot{n}_{H2} + \Delta S_{H2O}\dot{n}_{H2O} - \Delta S_{O2}\dot{n}_{O2} \tag{25}$$

This ARR can be used to monitor a fault in the cooling system, which is out of the scope of this paper.

4.2. Generation of robust adaptive thresholds

In principle, the robust ARRs can be generated from BG-LFT as detailed in Mohand Arab Djeziri et al. (2007, 2009, 2011). The procedure is not detailed in this paper. Moreover, as the interest of this paper doesn't lie in diagnosis of PEMFC *per se*, BG-LFT model of PEMFC is not developed here. Instead, BG-LFT model of EE subsystem is built for the robust detection of degradation-beginning. Consider BG-LFT model of EE subsystem, wherein the resistance element $R : Rh_{ohm}$ is considered as an uncertain parameter (cf. (26)). The multiplicative uncertainty $\delta_{Rh_{ohm}}$ related to additive uncertainty ΔRh as shown in (27).

$$Rh_{ohm} = Rh_{ohm,n}(1 + \delta_{Rh_{ohm}}) \tag{26}$$

$$\delta_{Rh_n} = \pm\Delta Rh / Rh_n \tag{27}$$

Consider ARR_2(see (22)) derived from energetic interaction present in the electrochemical subsystem, ARR_2 can be decoupled into nominal part $r_{2,n}(t)$ and uncertain part $r_{2,unc}$ as,

$$\begin{aligned} ARR_2 &= r_{2,n}(t) + r_{2,unc}(t) \\ &= \underbrace{n_s\left(E_0 - (R_{ohm,n})I_{fc} - ATln\left(\frac{I_{fc}}{I_0}\right) - BTln\left(1 - \frac{I_{fc}}{I_l}\right)\right) - SSe : U_{fc}}_{r_{2,n}(t)} - \underbrace{n_s\left(\delta_{Rh_{ohm}} Rh_{ohm,n} I_{fc}\right)}_{r_{2,unc}(t)} \end{aligned} \tag{28}$$

The uncertain part is used to form the thresholds as,

$$-a < r_{2,n}(t) < a \tag{29}$$

$$a = |w_{R_{ohm}}| = n_s|\delta_{Rh_{ohm}} Rh_{ohm,n} I_{fc}| \tag{30}$$

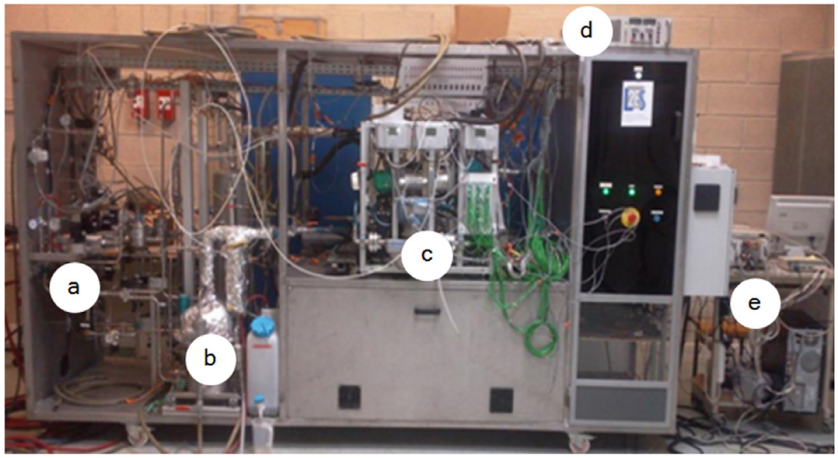

Fig. 3. 10 kW in-lab test bench: (a) air and hydrogen supplies, (b) humidifiers, (c) cooling system (the PEMFC is located behind), (d) electrical load, (e) control and acquisition unit.

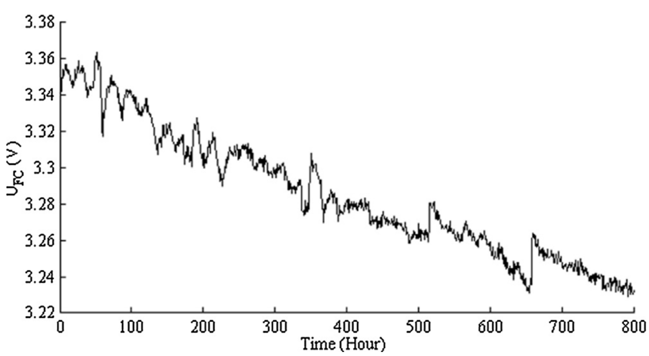

Fig. 4. Recorded voltage for FC1.

Table 1
Operating Conditions.

Parameter	FC1	FC2
Number of cells,n_s	5	8
Surface	100 cm^2	220 cm^2
Temperature, T	60 °C	80 °C
Anode and cathode stoichiometry ratios	1.5–2	1.5–2
Absolute pressure anode/cathode,P_{H2}& P_{O2}	1.5 bar	1.5 bar
Relative humidity anode/cathode	50%	50%
Nominal current, I_{nom}	70 A	100 A
Maximal current I_{max}	140 A	170 A

5. Degradation tests and degradation model

This section describes the industrial PEMFC setup and aging tests performed to obtain an appropriate DM.

5.1. Experimental setup

Degradation tests are carried out on a 10 kW test bench as shown in Fig. 3, which regulates the temperature (by means of a cooling system (c)), the moisture content (through boilers (b)), the anode and cathode pressures (through the air and hydrogen supplies (a)), the electrical load (d) and the test bench adjusts the gas flow rates accordingly. The stack voltages are recorded continuously (through the acquisition unit (e)) during the test with a one-hour sampling period.

5.2. Degradation tests

Two different type of degradation tests were performed:

Constant Load Test (referred to as FC1): This test is done for about 800 h, on a commercially available stack of 5 cells, surface of 100 cm^2 and a nominal current I_{nom} of 70A. This corresponds to the fuel cell one (FC1).

Variable Load Test (referred to as FC2): This test is done on a 8-cells stack PMFC with a surface of 220 cm^2, provided by the French Atomic Energy and Alternative Energy Commission (CEA). It is subjected to a μ-CHP profile (Combined Heat and Power) for a period of 900 h. This profile is designed to simulate the energy consumption of a building along a year and follows the seasons:

- Winter: I_{max} for about 250 h.
- Spring: 7 cycles of 24 h between I_{nom} and $I_{nom}/2$, followed by $I_{nom}/2$ until 500 h.
- Summer: $I_{nom}/2$ for 100 h, followed by 9 cycles of 24 h between $I_{nom}/2$ and null power demand until $t = 800$ h.
- Autumn: $I_{nom}/2$ until the end of the test.

The operating conditions of these two PEMFC are summarized in Table 1.

5.3. Degradation model

Although, it is possible to mathematically model the degradation physics (for instance, the loss of catalytic activity), in general, obtaining a physics based degradation model is a difficult task in the PEMFC context. The latter is caused due to huge variations in the degradation processes as most FCs are handmade. As such, degradation physics is sensitive to the quality of materials and gases used. Moreover, as of now, correlation of the physics based degradation models with experimental data is difficult. For instance, it is impossible to obtain measurements of the ECSA, compression of the Gas Diffusion Layer (GDL), and ionic resistance of the membrane. These measurements can be performed only after PEMFC has been dissembled.

On the other hand, the stack voltage can be measured easily to obtain statistical degradation models. Moreover, the stack voltage values represent the energetic assessment of the EE subsystem, to which the parametric degradations can be correlated. Periodically throughout the life of the fuel cell, the static response is measured with a polarization curve (voltage as a function of the current) as shown in (31). Note that ARR_2 derived in (22) is nothing but the polarization curve shown in (31), wherein the voltage sensor U_{fc} is

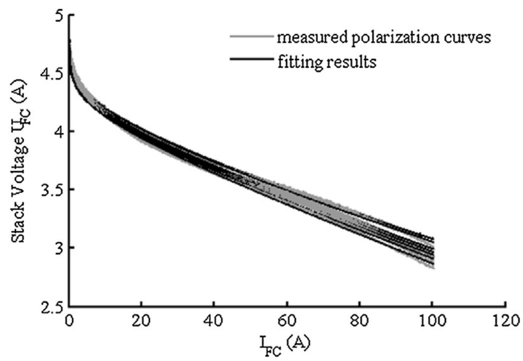

Fig. 5. Polarization Curve and fitting result during aging for FC1.

dualized to $SSe : U_{fc}$ to felicitate the derivation of ARR_2 (22). Thus, ARR_2 expression is used to obtain the polarization curve as,

$$U_{fc} = n_s \left(E_0 - Rohm I_{fc} - AT \ln\left(\frac{I_{fc}}{I_0}\right) - BT \ln\left(1 - \frac{I_{fc}}{I_L}\right)\right) \quad (31)$$

At each characterization time, Levenberg-Marquardt method is used to extract the parameters of (26). The algorithm is initiated with a set of parameters whose values are chosen from the literature (Laffly et al., 2007; Larminie et al., 2003). The algorithm extracts: the Open Circuit Voltage (OCV) E_0 at nominal pressure and temperature, the global resistance *Rohm* (membranes, connectors, end plates, etc.), the exchange current I_0 and the limiting current I_L.

5.3.1. Constant load tests (FC1)

With nominal current of 70 A, the recorded stack voltage U_{fc} (at sampling period of one Hour) is shown in Fig. 4.

Then, model fitting of the measured polarization curves (during aging) is shown in Fig. 5. Fig. 6 shows the evolution of the parameter value with respect to the initial one (in percentage). From the four chosen parameters, only two show significant deviations: the overall resistance *Rohm* increases by more than 12% while the limit current I_L decreases by 13%.

5.3.2. Variable load (FC2)

The current load profile and the corresponding recorded voltage for FC2 is shown in Fig. 7. The corresponding polarization curve is shown in Fig. 8.

The evolution of extracted parameters is shown in Fig. 9. Significant deviations are visible in: i) the overall resistance *Rohm* which increases by more than 70%; ii) the limit current I_L that decreases by 60%. As observed for both FC1 and FC2, only two parameters *Rohm* and I_L show significant deviation over their initial values. Change in *Rohm* is mainly due to degradation and dehydration of the polymer membrane and the corrosion of the carbon support for the resistance (Fowler et al., 2002). The limit current decreases due to the ripening of the catalyst particles, an insufficient evacuation of the water (due to changes in the surface) and the compression of the GDL (Schmittinger and Vahidi, 2008). There is no significant evolution in the value of the OCV and the exchange current I_0, compared to the other parameters. Therefore, OCV and I_0 are considered constant.

For a given operating condition, since only the stack voltage is measured, it is impossible to separate the mutual coupling of global resistance and limiting current i.e. the loss due to both of the phenomena is not observable simultaneously. Moreover, although not perfectly, both *Rohm* and I_L seem to evolve in an approximate linear fashion. Therefore, the variations in the latter are parameterized with a single parameter α, a State of Health (SOH) indicator (not to be confused with $\alpha - \lambda$ metric, see Section 7). The parametric variation is expressed through a linear model as,

$$R_{ohm}(t) = R_{ohm,n}(1 + \alpha(t)) \quad (32)$$

$$I_L(t) = I_{L,n}(1 - \alpha(t)) \quad (33)$$

$$\alpha(t) = \beta \times t \quad (34)$$

where β explains the rate of change of α and sub-script n denotes the nominal value. Very recently, a similar approach has been followed in Bressel et al. (2016a) for construction of DM. In this work, SOH is assessed with respect to state of α and β.

5.4. Remark

The phenomenon of voltage drop following a linear-logarithmic relation is admitted by the fuel cell community (Jouin et al., 2014a; Kundu et al., 2008). In our context, with linear evolution of the SOH indicator α, the voltage drop follows a linear-log relation (see (26)). Here, linear voltage drop is due to increase in membrane resistivity and logarithmic part is caused by increase in concentration/diffusion losses. The latter is significantly related with deviation in limiting current (Kundu et al., 2008).

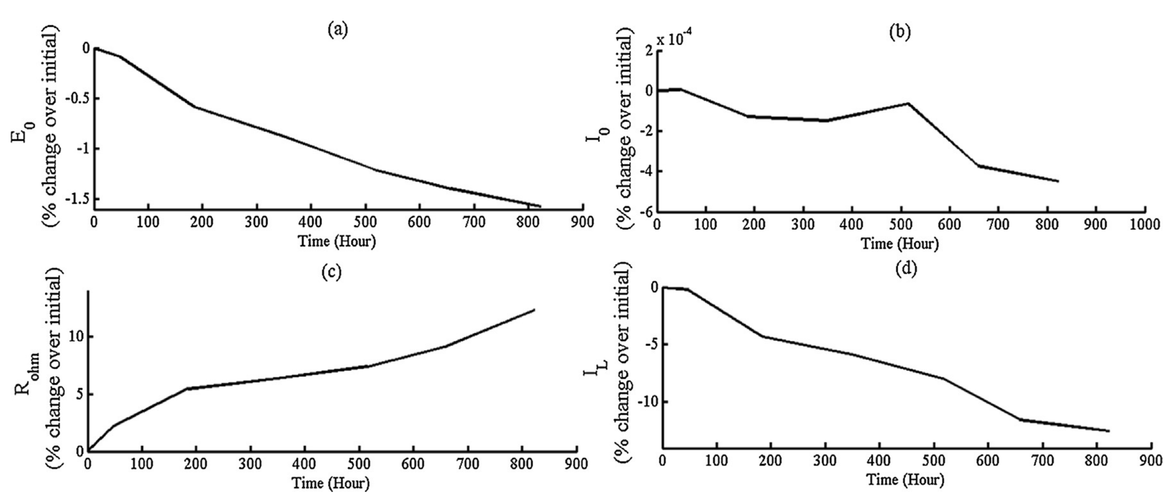

Fig. 6. Case FC1: Deviation of the parameters values (in percentage of their initial value) during aging: (a) Change in E_0, (b) Change in I_0, (c) Change in R_{ohm} (d) Change in I_L.

Please cite this article in press as: Jha, M.S., et al., Particle filter based hybrid prognostics of proton exchange membrane fuel cell in bond graph framework. Computers and Chemical Engineering (2016), http://dx.doi.org/10.1016/j.compchemeng.2016.08.018

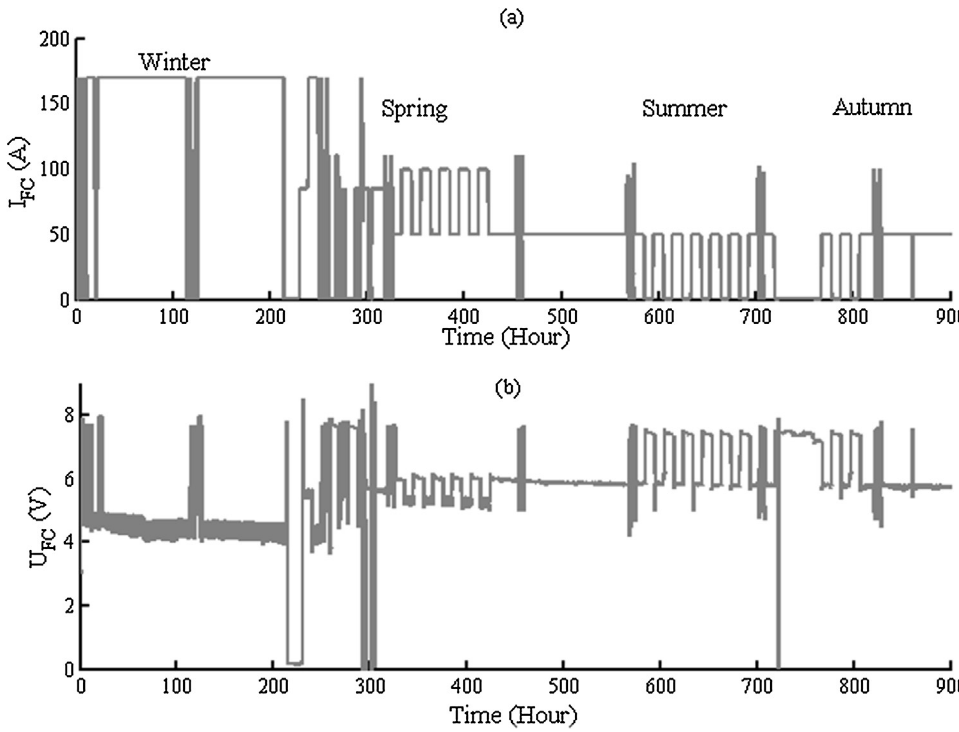

Fig. 7. Recorded profile for FC2: (a) Current (Load) Profile (b) Recorded Voltage.

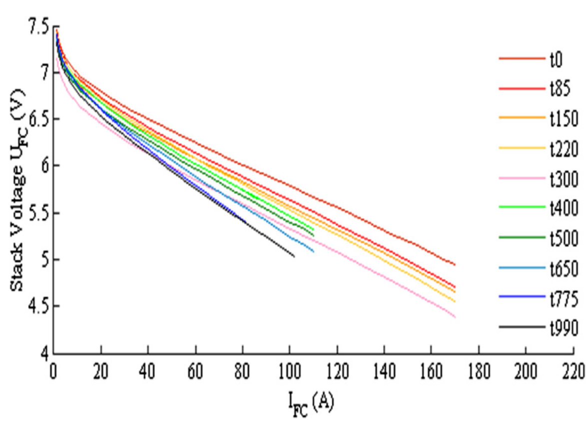

Fig. 8. Polarization curves during aging for FC2.

5.4.1. *Degradation model*

SOH indicator α is chosen as *prognostic candidate* with respect to which, RUL predictions are generated. β influences the speed of degradation; as such, it is considered as the *degradation progression parameter* (DPP) (M. S. Jha et al., 2016). DM is inspired from statistical evolution of *Rohm* and I_L (see (32)-(34)) as,

$$\alpha(t) = \beta(t) \times t + \upsilon \tag{35}$$

where $\upsilon \sim \mathcal{N}(0, \sigma_\upsilon^2)$ is the associated process noise.

6. Hybrid prognostics

In this section, the hybrid prognostics methodology proposed in Jha et al. (2016) is applied in the PEMFC context. However, instead of building uncertain BG model with interval valued uncertainties, BG-LFT model (see Fig. 2) is exploited for robust detection of degradation initiation. It should be noted that although the DM model is obtained in a statistical way, the measurement of the degradation is obtained from BG model based power conservative ARR.

6.1. *Fault model*

The *prognostic candidate* is included as a tuple (α, β) to construct a *fault model* in state space form.

6.1.1. *State equation*

In discrete time $k \in \mathbb{N}$, state equation is inspired from DM (see (35)) as,

$$\alpha_k = \alpha_{k-1} + \beta_{k-1} \times \Delta t + \upsilon_{k-1} \tag{36}$$

$$\beta_k = \beta_{k-1} + \xi_{k-1} \tag{37}$$

where, $\upsilon_k \sim \mathcal{N}(0, \sigma_\upsilon^2)$ is the associated process noise, hidden DPP β is modeled as random walk process, $\xi_k \sim \mathcal{N}(0, \sigma_\xi^2)$ is random walk noise and Δt is the sample time. The state transition dynamics is assumed to follow first order Markov dynamics.

6.1.2. *Observation equation*

The observation equation relates the degradation information with the state variables α and β. ARR_2 (see (28)) corresponds to energetic assessment in EE subsystem; as such, it remains sensitive to R_{ohm} and I_L. With suitable algebraic manipulations, nominal part of an uncertain ARR can be exploited to obtain state information (Jha et al., 2016). In this manner, detection of degradation commencement and prognostics can be achieved in a unified way. To this end, ARR_2 is expressed as,

$$ARR_2 : r_2(t) = n_s\left(E_0 - \left(R_{ohm,n}\left(1+\alpha(t)\right)\right)I_{fc} - ATln\left(\frac{I_{fc}}{I_0}\right)\right.$$
$$\left.-BTln\left(1 - \frac{I_{fc}}{I_{L,n}\left(1-\alpha(t)\right)}\right)\right) - SSe : U_{fc} = r_{2,n}(t)$$

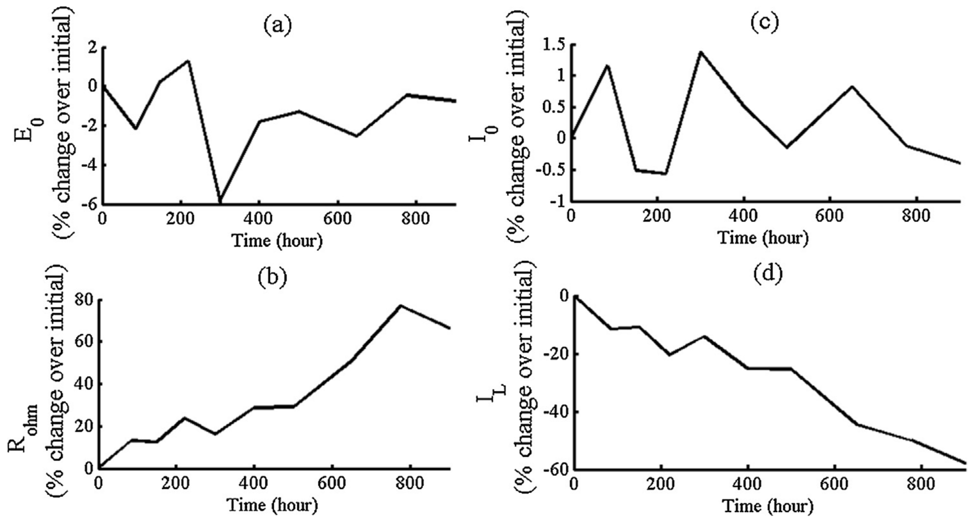

Fig. 9. Case FC2: Derivation of the parameters values (in percentage of their initial value) during aging: (a) Change in E_0, (b) Change in I_0, (c) Change in R_{ohm} (d) Change in I_L.

$$+n_s\left(-R_{ohm,n}\alpha(t)I_{fc}-BTln\left(1-\frac{I_{fc}}{I_{L,n}(1-\alpha(t))}\right)\right.$$
$$\left.+BTln\left(1-\frac{I_{fc}}{I_{L,n}}\right)\right) \qquad (37)$$

$\forall t>0$, power conservation in ARR dictates,

$$r_2(t)=r_{2,n}(t)+n_s\left(-R_{ohm,n}\alpha(t)I_{fc}-BT\ \ ln\left(1-\frac{I_{fc}}{I_{L,n}(1-\alpha(t))}\right)\right.$$
$$\left.+BT\ \ ln\left(1-\frac{I_{fc}}{I_{L,n}}\right)\right)=0 \qquad (37)$$

Thus, measurement of $\alpha(t)$ can be acquired from $r_{2,n}(t)$. In discrete time k, observation equation is built as,

$$y^d(k)=r_{2,n}(k)=n_s\left(R_{ohm,n}\alpha_k I_{fc}+BT\ \ ln\left(1-\frac{I_{fc}}{I_{L,n}(1-\alpha_k)}\right)\right.$$
$$\left.-BT\ \ ln\left(1-\frac{I_{fc}}{I_{L,n}}\right)\right)+w_k^d \qquad (37)$$

where $w_k^d\sim N(0,\sigma_{w^d}^2)$ models the noise associated with residual measurements. It is considered additive, *independent and identically distributed* (i.i.d.) drawn from a zero mean normal distribution, assumed to be uncorrelated to state process.σ_{w^d} is approximated from residual measurements during degradation tests.

6.2. Particle filter based SOH estimation and RUL prediction

The RUL predictions are obtained on the basis of actual SOH estimate which are in turn achieved using Bayesian inference. The Bayesian solution to the problem of $\alpha_k,\ \ \beta_k$ estimation at discrete time k, based upon the history of measurements till time k, $y^d_{0:\ k}$, is formulated as state-parameter joint estimation problem in PF framework. The SOH estimate is obtained in form of probability density function (PDF)$p(\alpha_k,\ \ \beta_k|{y^d}_{0:\ k})$. The arriving measurement ${y^d}_k$, is assumed conditionally independent of the state process. The likelihood function becomes as,

$$p\left(y_k^d|\alpha_k,\ \ \beta_k\right)=\frac{1}{\sigma_{w_k^d}\sqrt{2\pi}}\exp\left(-\left(y_k^d-h^d\left(\alpha_k,\ \ \beta_k\right)\right)^2/2\sigma^2_{w_k^d}\right) \qquad (38)$$

where $h^d(.)$ is any non-linear function constituting the observation equation (32). Given the *prior* PDF $p(\alpha_k,\ \ \beta_k|{y^d}_{0:\ k-1})$, Bayes rule is applied to update the *prior* as the measurement arrives (Arulampalam et al., 2002). The latter gives the *posterior* PDF of degradation state $p(\alpha_k,\ \ \beta_k|{y^d}_{0:\ k})$. However, the recursive computation of *posterior* involves an integral due to which, in general, closed form solutions cannot be obtained. Thus, one resorts to Monte Carlo sampling based PF where the state PDF is approximated by set of discrete weighted samples or particles, $\{(\alpha_k^i,\ \ \beta_k^i),\mathrm{w}_k^i\}_{i=1}^N$, where N is the total number of particles. For i^{th} particle at time k, $\alpha_k^i,\ \ \beta_k^i$ are the joint estimate of the state. In PFs, the posterior density at any time step k is approximated as,

$$p(\alpha_k,\ \ \beta_k|y^d_{0\ :\ k})\approx\sum_{i=1}^N \mathrm{w}_k^i.\delta_{(\alpha_k^i,\beta_k^i)}(d\alpha_k^i\ \ d\beta_k^i) \qquad (39)$$

where $\delta_{(\alpha_k^i,\beta_k^i)}(d\alpha_k^i\ \ d\beta_k^i)$ denotes the Dirac delta function located at $(\alpha_k^i,\ \ \beta_k^i)$ and sum of the weights $\sum_{i=1}^N \mathrm{w}_k^i=1$. In this paper, PF is not described; it can be found well detailed in Arulampalam et al. (2002).

6.2.1. State of health estimation

In this work, *sampling importance resampling* (SIR) PF is employed owing to the easiness of *importance weight* evaluation (Arulampalam et al., 2002). Firstly, it is assumed that the set of random samples (particles) $\{(\alpha_{k-1}^i,\ \ \beta_{k-1}^i),\mathrm{w}_k^i\}_{i=1}^N$ are available as the realizations of posterior probability $p(\alpha_{k-1}^i,\beta_{k-1}^i|y^d_{0\ :\ k-1})$ at time $k-1$. Then, three main steps are followed as illustrated in Fig. 10.

6.2.1.1. Prediction. The particles are propagated through system model by: sampling from the system noise υ_{k-1} and simulation of system dynamics (see (31),(32)), as illustrated in Fig. 10. This leads to new set of particles which are the realizations of prediction distribution $p(\alpha_k,\beta_k|y^d_{0\ :\ k-1})$.

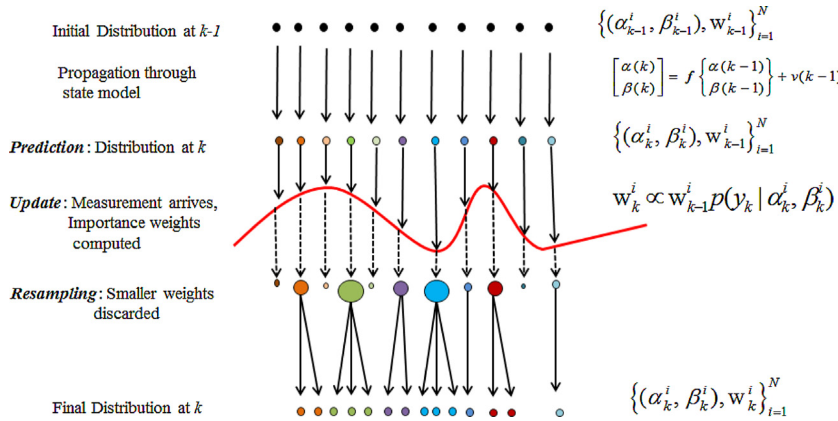

Fig. 10. Illustration of estimation process in Particle Filters.

6.2.1.2. Update. As the new measurement y_k^d arrives, a weight w_k^i is associated to each of the particles based on the likelihood of observation y_k^d made at time k:

$$w_k^i = p(y_k^d|\alpha_k^i, \beta_k^i) / \sum_{j=1}^{N} p(y_k^d|\alpha_k^j, \beta_k^j) \tag{40}$$

6.2.1.3. Resampling. Previous steps lead to a situation where the importance weights become increasingly skewed. After few iterations, all but one particle have negligible weights (particle *degeneracy*) (Doucet and Johansen, 2009). To avoid the latter, a new swarm of particles are resampled from the approximate *posterior* distribution obtained previously in the *update* stage, constructed upon the weighted particles. The probability for a particle to be sampled remains proportional to its weight. This way, particles with smaller weights (signifying less contribution to estimation process) are discarded and particles with large weights are used for resampling (see Fig. 10). In this work, *systematic resampling* is preferred owing to its simplicity in implementation, $O(N)$ computational time and modular nature. Being modular in nature, the algorithm code can be simply injected into the main procedure. In this paper, *systematic resampling* algorithm as given in Arulampalam et al. (2002) has been implemented.

The *prediction*, *update* and *resample* procedures form a single iteration step; they are applied at each time step k.

6.2.2. RUL prediction

The critical/failure value α_{fail} must be decided beforehand. Once the *posterior* PDF $p(\alpha_k, \beta_k|y_{0:k}^d)$ has been estimated at time step k, it can be projected in future such that information about EOL at time step k, EOL_k is obtained depending upon the actual SOH. Then, RUL at time k, can be obtained as,

$$RUL_k = EOL_k - k \tag{41}$$

Obviously, such a projection of degradation trajectory in future has to be done in absence of measurements. As illustrated in Fig. 11, in order to achieve such a projection, *posterior* $p(\alpha_k, \beta_k|y_{0:k}^d)$ can be propagated using state model (36) until the failure horizon α_{fail} is reached. The latter may take l^d time steps so that $\alpha \geq \alpha_{fail}$ at a time $t + l^d$. This calls for computation of the predicted degradation state $p(\alpha_{k+l^d}, \beta_{k+l^d}|y_{0:k}^d)$ as (Doucet et al., 2001):

$$p(\alpha_{k+l^d}, \beta_{k+l^d}|y_{0:k}^d) = \int \cdots \int \prod_{j=k+1}^{k+l^d} p\left(\left(\alpha_j, \beta_j\right) | \left(\alpha_{j-1}, \beta_{j-1}\right)\right) \; p(\alpha_k, \beta_k|y_{0:k}^d) \prod_{j=k}^{k+l^d-1} d\left(\alpha_j, \beta_j\right) \tag{42}$$

In PF framework, (37) can be evaluated by propagating each of the particles $\left\{(\alpha_k^i, \beta_k^i), w_k^i\right\}_{i=1}^{N}$ constituting $p(\alpha_k, \beta_k|y_{0:k}^d)$, l^d-step ahead into future (Daigle and Goebel, 2010; Jouin et al., 2014a). Here, $l^d = 1, \ldots T^d - k$, where T^d is the time until SOH remains lesser than failure value i.e. time until $\alpha_{k+l^d} \geq \alpha_{fail}$. Each of the particles is propagated using the state equation (31). In this paper, for the i^{th} particle, the corresponding weight during the $l^{d,i}$-step propagation is kept equal to weight w_k^i at time of prediction k. This is based upon the assumption that error generated/accumulated by keeping the weights same, is negligible compared to other error sources, such as settings of process noise, measurement noise, random walk variance, model inaccuracy etc. (Orchard, 2007). Then, for i^{th} particle, $RUL_k^i = k + l^{d,i} - k = l^{d,i}$ and the corresponding PDF is obtained as,

$$p(RUL_k|y_{0:k}^d) \approx \sum_{i=1}^{N} w_k^i \;\; \delta_{(RUL_k^i)}(d\,RUL_k^i) \tag{43}$$

The pseudo algorithm for SOH estimation and RUL prediction is shown in Table 2.

7. Evaluation metrics

Various metrics employed to evaluate the prognostic performance are briefly discussed. Readers are referred to Saxena et al. (2010) for details and Daigle and Goebel, (2010), Daigle and Goebel, (2013) for the implementation of the same. Root mean square error (RMSE) metric expresses the relative estimation accuracy as:

$$\mathrm{RMSE}_X = \sqrt{Mean_k \left[\left(\frac{mean(X) - X^*}{X^*} \right)^2 \right]} \tag{44}$$

where, for species X, X^* denotes the corresponding true values. $Mean_k$ denotes the mean over all values of k. At a particular prediction instant k, the prediction accuracy is evaluated by relative accuracy (RA) metric as,

$$\mathrm{RA}_k = \left(1 - \frac{|RUL_k^* - \mathrm{Median}\,p(RUL_k)|}{RUL_k^*} \right) \tag{45}$$

$$\overline{\mathrm{RA}} = \mathrm{Mean}_k p(\mathrm{RA}_k) \tag{46}$$

where RUL_k^* denotes the true RUL at time k. The overall accuracy is determined by $\overline{\mathrm{RA}}$ as shown in (40), where RA_k is averaged over all the prediction points. Moreover, $\alpha - \lambda$ metric (Saxena et al., 2010), is used to assess the RUL prediction performance. Here, $\alpha \in [0, 1]$ defines the bounds of true RUL as $(1 \pm \alpha)RUL_k^*$. The third parameter

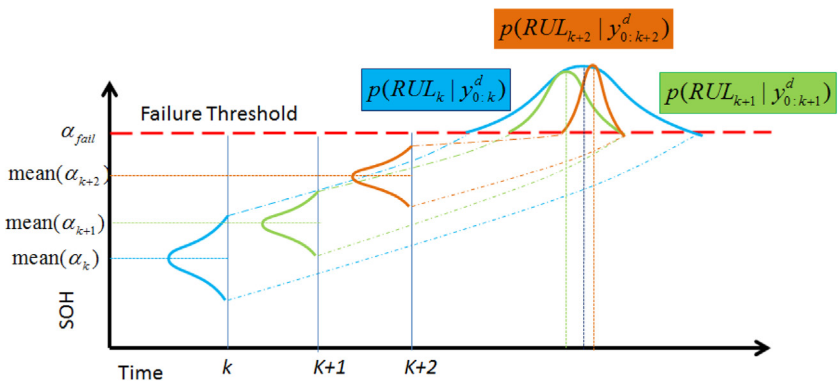

Fig. 11. Schematic illustration of RUL prediction process.

Table 2
SOH Estimation and RUL Prediction using SIR PF.

Algorithm: SOH estimation and RUL Prediction for FC1 and FC2

Inputs: $\left\{(\alpha_{k-1}{}^{,i},\ \beta_{k-1}{}^{,i}), w^i_{k-1}\right\}_{i=1}^{N}, r_{2,n}$
Variable: l
Output: $\left\{(\alpha_k{}^{,i},\ \beta_k{}^{,i}), w^i_k\right\}_{i=1}^{N}; p(RUL_k|r_{2,n})$
% SOH Estimation
for $i = 1$ **to N do**
$\beta_k{}^{i} \sim p(\beta_k{}^{,i}|\beta^i_{k-1})$
$w^i_k \sim p(y^d_k|\alpha^i_k, \beta^i_k)$
end for
$W \longleftarrow \sum_{i=1}^{N} w^i_k$
for $i = 1$ **to N do**
$w^i_k \longleftarrow w^i_k/W$
end for
$\left\{(\alpha_k{}^{,i},\ \beta_k{}^{,i}), w^i_k\right\}_{i=1}^{N} \longleftarrow \text{RESAMPLE}\left\{(\alpha_k{}^{,i},\ \beta_k{}^{,i}), w^i_k\right\}_{i=1}^{N}$
% RUL Prediction
for $i = 1$ **to N do**
$l = 0$
while $\alpha^i_{k+l} \le \alpha_{fail}$ **do**
$\beta^i_{k+1} \sim p(\beta^i_{k+1}|\beta^i_k)$
$\alpha^i_{k+1} \sim p(\alpha^i_{k+1}|\alpha^i_k, \beta^i_{k+1})$
$l \longleftarrow l + 1$
end while
$RUL^i_k \longleftarrow l$
end for
$\left\{RUL^i_k, w^i_k\right\}_{i=1}^{N} \sim p(RUL_k|r_{2,n})$

$\beta \in [0, 1]$ signifies the desired (pre-fixed) fraction of the RUL prediction probability mass percentage that should fall between the cones of accuracy determined by α, for the respective RUL prediction to be acceptable.

8. Results

The BG-LFT derived thresholds (see (23)-(25)) are used to detect the initiation of degradation, when the ohmic resistance exceeds its permissible deviation limits. Once the degradation is detected, the estimation and RUL prediction process is triggered.

8.1. Constant load (FC1)

Motivated from Fig. 6, $\alpha_{fail} = 0.12$ signifies EOL of FC1 with 12% deviation on initial value. Moreover, the true value of α,α_{true} is considered to evolve in a perfect linear way with true value of slope β, $\beta_{true} = 1.3 \times 10^{-4}$. Thus, α_{fail} is reached at 900 h. Value of the measurement noise variance σ^2_{wd} is obtained from square of the standard deviation of the nominal residual $r_{2,n}$ recorded during degradation tests, as $\sigma^2_{wd} = 10^{-6}$.

8.1.1. PF settings

Estimation performance by PF (see Fig. 12), is realized with N = 2000 particles. The measurement noise variance in PF is set as 100 times that of residual measurement variance σ^2_{wd}. This is done to ensure a good estimation of the noisy measurement throughout (M. J. Daigle and Goebel, 2013). The initial random walk noise variance is set as, $\sigma^2_{\xi} = 10^{-10}$ for a quick convergence. A good value for process noise variance is found through successive tuning as $\sigma^2_{v} = 10^{-6}$, to obtain a smooth desirable estimation. As shown in Fig. 12c, degradation is detected at $t = 58$ h by thresholds triggering the prognostic module. The thresholds a and $-a$, are sensitive to 2% uncertainty over nominal Rh_{ohm} i.e. $\delta_{Rh_{ohm}} = \pm 2\%$ Rh_{ohm} and the constant I_{fc}(cf. (25)). The measurement signal $r_{2,n}(t)$ is estimated with $RMSE_{r_{2,n}} = 4.2\%$. This way, the non-linearity that locally manifests in the residual is accurately estimated.

8.1.2. SOH estimation

Fig. 12a shows the estimation of fairly linear α with $RMSE_{\alpha} = 23.56\%$.β remains fairly constant; it is estimated accurately with $RMSE_{\beta} = 9.3\%$.

8.1.3. RUL predictions

Fig. 13 shows the box plots of RUL prediction obtained at time intervals of 25 h (for the sake of clarity). For all time points, prediction performance is assessed using α-λ metric with $\alpha = 0.4$ and

Table 3
Estimation-Prediction Performance Under With Different Number of Particles.

N	$RMSE_{r_{2,n}}$	$RMSE_{\alpha}$	$RMSE_{\beta}$	$\overline{\text{RA}}$	Computation Time Taken for First Prediction Step	Total Computational Time for Prediction
100	9.03%	31.43%	22.3%	68.54%	14.56 s	6.45 min
500	7.56%	28.67%	17.78%	76.56%	1 min 34 s	1 h 34 min
1000	6.84%	25.43%	11.44%	89.43%	2 min 28 s	3 h 31 min
2000	4.2%	23.56%	9.3%	96.07%	4 min 5 s	6 h 48 min

Please cite this article in press as: Jha, M.S., et al., Particle filter based hybrid prognostics of proton exchange membrane fuel cell in bond graph framework. Computers and Chemical Engineering (2016), http://dx.doi.org/10.1016/j.compchemeng.2016.08.018

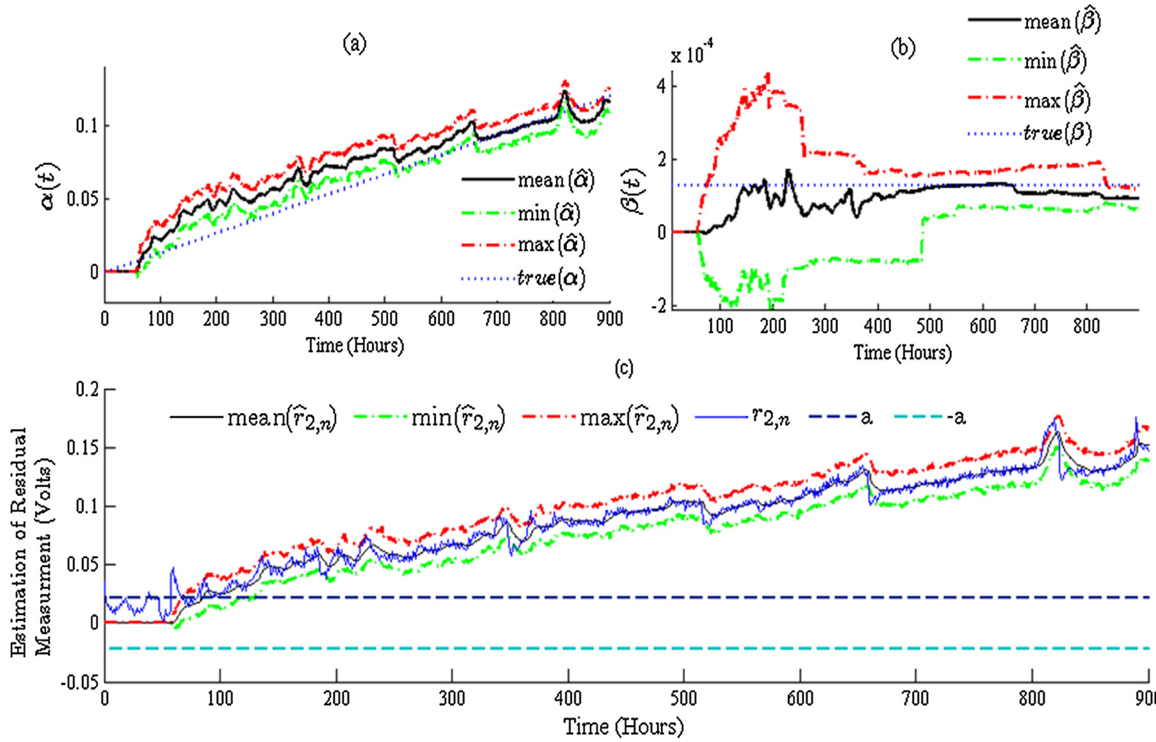

Fig. 12. Estimation performance in PF for FC1 (a). Estimation of α (b) Estimation of β.(c) Measurement via. residual and its estimation.

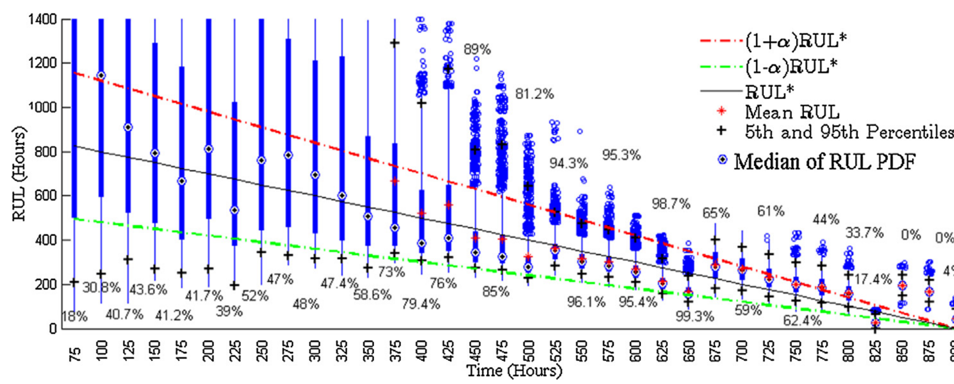

Fig. 13. RUL prediction in PF for FC1.

$\beta = 0.4$. The latter implies a requirement of 40% of RUL probability mass containment within 40% of true RUL value, for the RUL prediction to be considered viable. The percentage of probability mass falling within the accuracy cone is indicated against each box plot. Starting from $t = 200$ h, almost all the predictions are *true* (acceptable), except the ones at the last four prediction-points. This mainly arises due to characterizations performed at $t = 800$ h, so that an insufficient recovery effect manifests on the stack voltage while the latter is being recorded. Over all, starting from $t = 350$ h, the prediction performance is very good with $\overline{RA} = 96.07\%$.

As shown in Table 3, with various PF factors kept same, an increase in number of PF particles leads to efficient measurement estimation and prediction accuracy. This justifies the choice $N = 2000$, implemented in this paper. During RUL prediction, each of the particles is propagated into future. As such, computational complexity is: i) directly related to number of particles used, ii) inversely related to the time instant (from start) at which RUL prediction is made. It also depends upon estimation values of hidden DPPs (M.J. Daigle and Goebel, 2013). This is clearly reflected in Table 3. Computational time per sample step usually decreases as the time of prediction nears the end of life. In fact, larger the number of particles employed, higher is: i) estimation efficiency, ii) RUL prediction efficiency, iii) consumption of total computational time. These 900 h of data were run on an Intel Core i7 Processor with 16 GB RAM and 2.30 GHz clock frequency. The total time taken for prediction was 6 h 48 min (see Table 3).

8.1.4. Discussion

With real experimental data at hand, in reality, α_{true} is only approximately linear and β_{true} is never perfectly constant. As such, $RMSE_\alpha$ and $RMSE_\beta$ cannot be regarded as reliable metrics for evaluation of estimation performance. However, $RMSE_{r2,n}$ rightly indicates the accuracy of measurement estimation. Moreover, prediction performance is accurately judged by $\overline{RA}$ metric as the speed of degradation is uniform (constant loading regime).

Performance comparison: Recently, Bressel et al. (2016a) obtained the SOH estimations using Extended Kalman Filter (EKF) (Celaya et al., 2011; Haykin, 2004), exploiting the same degradation

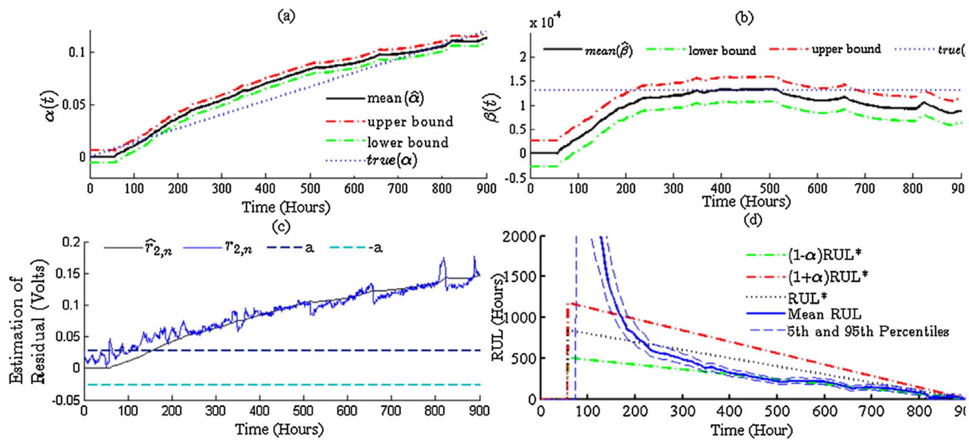

Fig. 14. Estimation and RUL prediction by EKF for FC1 (a). Estimation of α (b) Estimation of β. (c) Measurement via. residual and its estimation (d) RUL Prediction.

Table 4
Performance comparison with Extended Kalman Filter.

Estimator	$RMSE_{r_{2,n}}$	$\overline{\text{RA}}$	Total Computational Time for Prediction
PF (N = 2000)	4.20%	96.07%	6 h 48 min
EKF	9.86%	38.16%	Around 5 s

Table 5
Standard deviation & RMSE of Residual measurements.

Time	Standard Deviation of Measurement (Residual $r_{2,n}$)	$RMSE_{r_{2,n}}$
100 < t < 300 h	0.156 V	42.56%
300 < t < 570 h	0.0532 V	19.56%
570 < t < 820 h	0.0145 V	6.85%
820 < t < 900 h	0.0136 V	1.54%

data set. For a comparative study, the methodology implemented here is replaced with EKF as the Bayesian estimator. A total of 20 simulations are performed with different settings of EKF parameters. The results are shown in Fig. 14.

With EKF as the estimator, the bounds on RUL are obtained using the Inverse First Order Reliability Method (IFORM) (Hohenbichler et al., 1987), which is used to estimate unknown parameters (for instance, the RUL) for a specified failure probability level (Bressel et al., 2016).

As observed in Table 4, although the sub-optimal EKF gives a manageable $RMSE$, the associated $\overline{\text{RA}}$ (considering the mean of RUL's PDF) is comparatively very low. Moreover, there is a huge difference in the computational time. Thus, EKF may be employed where computation time is the major concern. As prognostic issues are majorly dealt in an offline manner, PF outperforms EKF and promises better prognostic outputs. Moreover, EKF may not be the best choice of the estimator when degradation models are highly non-linear (like crack propagation etc. (Zio and Peloni, 2011)). The latter, however, can be well taken care by PF.

8.2. Variable load (FC2)

Motivated from Fig. 9, $\alpha_{fail} = 0.6$ signifies end of life of FC2 with 60% of deviation on its initial value. In the variable load regime, the varying current profile (see Fig. 7) mimics the PEMFC usage in different seasons. Variable load profile affects the speed of degradation significantly. As such, α_{true} seems to evolve in a piece-wise linear manner (see Fig. 9(b) and (d)). In fact, α_{true} and β_{true} are unknown in reality. Moreover, measurements are severely affected by the characterizations (see Fig. 7(b) and Fig. 15. (c)), as re-standardizations of temperature conditions and evacuation of liquid water are done at each phase of characterizations. This is followed by recovery effects that enable a good SOH estimation.

PF settings: SOH estimations (see Fig. 15) are realized with N = 2000 PF particles. The initial measurements $r_{2,n}$ are heavily corrupted with noise and remain sensitive to stack voltage and current load. As such, the detection of degradation-beginning using BG-LFT thresholds is not viable. For this reason, the SOH estimations are triggered at initial time t = 0 h. Values of measurement noise variance σ^2_{wd} are obtained from square of the standard deviation of the nominal residual $r_{2,n}$ for various time regimes, as listed in Table 5. The measurement noise variance in PF is set as 100 times that of residual measurement variance σ^2_{wd}. This is done to ensure a good estimation throughout. The $RMSE_{r_{2,n}}$ for different time regimes are listed in Table 5. It should be noted that less $RMSE_{r_{2,n}}$ can be obtained with different PF settings; however, this may lead to non-smooth estimations of $\alpha(t)$ and $\beta(t)$ with very large spread and thus, non-viable RUL predictions.

SOH Estimation: Due to variable speeds of degradation, the reliable ground truths for evaluation of $RMSE_\alpha$ and $RMSE_\beta$ cannot be found. Thus, a quantitative comparison of estimation performance of $\alpha(t)$ and $\beta(t)$ cannot be made using $RMSE_\alpha$ and $RMSE_\beta$. However, qualitatively, the results are observed to be very satisfactory as $\hat{\alpha}$ reaches α_{fail} at EOL. The initial random walk noise variance is set as, $\sigma^2_\xi = 10^{-10}$ for a quick convergence. A good value for process noise variance is found through successive tuning as $\sigma^2_v = 10^{-5}$, to obtain the desirable estimation.

RUL Predictions: Box plots of RUL predictions are shown in Fig. 16. It should be noted that prediction accuracy in Fig. 13 (constant load case) is assessed by RUL*, α-λ and $\overline{\text{RA}}$ metrics. However, prediction accuracy Fig. 16 cannot be evaluated using the same metrics due to non-uniform rate of degradation. In Fig. 16, RUL predictions obtained until t = 475 h are virtually useless owing to their huge median value and large spread. This can be attributed to the large associated $RMSE_{r_{2,n}}$. However, after t = 475 h, useful predictions are obtained with small $RMSE_{r_{2,n}}$; this leads to efficient estimations of $\alpha(t)$, $\beta(t)$. The accuracy of RUL predictions is reflected by the fact that it converges to zero at its true EOL of 900 h. Moreover, at t = 800 h, the RUL seems to converge to value zero. This is in accordance with estimation of $\alpha(t)$ which seems to reach α_{fail} at t = 800 h, followed by recovery of SOH before the next characterization is performed (see Fig. 15. (c)). Clearly, the RUL distribution is assessed with very high accuracy and precise confidence bounds. Being run on the computer of same configuration as FC1, the RUL prediction took around 4 h 28 min of total computation time.

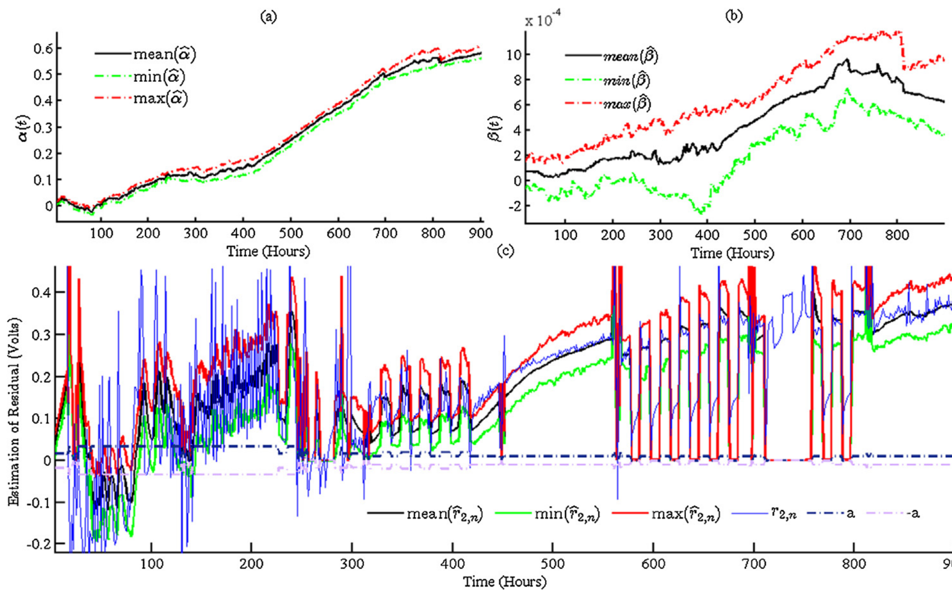

Fig. 15. Estimation performance in PF for FC2 (a). Estimation of α (b) Estimation of β.(c) Measurement and its estimation.

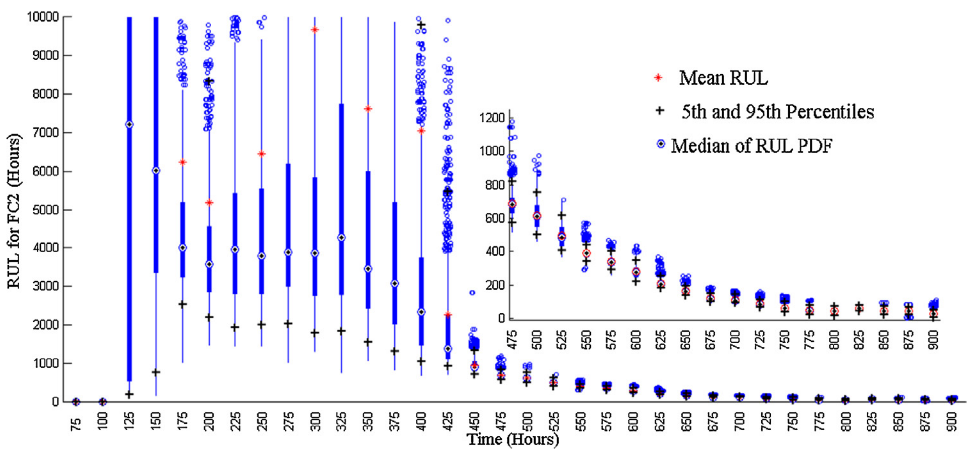

Fig. 16. RUL Prediction for FC2.

9. Conclusions

1 The BG model of PEMFC is developed in this work which presents a simplified graphical representation of the complex physics of PEMFC and efficient decomposition based upon functionality. Moreover, the model is well-suited for diagnostics and prognostics as a systematic derivation of fault indicators is achieved by exploiting structural and causal relationships. This BG model can further be used for prognostics of other sub-systems (hydraulic, thermal etc.) as the degradation data is procured or DMs become available. The latter forms a potential future work. Additionally, the exact knowledge of degradation commencement is essential for efficient prognostics. The BG LFT model constructed for the subsystem of interest provides the significant information of degradation-beginning through robust passive-type detection. This technique can be exploited as a diagnostic module in an integrated health monitoring framework or separately, over other subsystems in PEMFC context.

2 In this paper, the two degradation tests were performed under completely contrast situations (constant load and variable load solicitations), over two dimensionally different PEMFCs (FC1 and FC2). They have: (i) given similar degradation trend (ii) been successful in indicating the subsequent RUL for each case. As such, ohmic resistance and limiting current can be exploited as viable prognostics indicators. Moreover, the linear degradation model can be employed over similar PEMFCs with other machine learning techniques for prognostics.

3 It has been successfully shown that PF provides SOH estimations and RUL predictions with very high accuracy, accompanied with precise confidence bounds. Moreover, the RUL evaluation metrics employed in this paper are comprehensively much stricter than the existing PF based works (Jouin et al., 2014a,b, 2015), that employ PF for PEMFC prognostics. Additionally, the accuracy of PF is shown to be much higher than EKF, but with higher computational cost. Specifically, an approximate 96% of relative accuracy is achieved for RUL predictions under constant current solicitation. The PF computational time has been analyzed with different number of particles for 900 h of data, wherein maximum accuracy is achieved with an approximate total of 7 h of computational time. The latter signifies an effective 28 s of computation per hour. As such, PF can be used as a dedicated estimator in real time for prognostics. On the other hand, for variable current load case, the initial RUL predictions can be ameliorated through online standard deviation calculation of residual, adaptation of the random walk noise variance (Daigle and Goebel, 2013), and PF measurement variance etc. These issues shall be resolved in future works.

The accuracy of results obtained here demonstrates the viability of the method for prognostics. As such, this work forms a reliable reference for related future works and a significant contribution towards efficient prognostics in BG framework.

Acknowledgements

This work was supported by the project ANR PROPICE (ANR-12-PRGE-0001) and by the project LABEX ACTION (ANR-11-LABX-01-0) both funded by the French National Research Agency.

References

An, D., Kim, N.H., Choi, J.-H., 2015. Practical options for selecting data-driven or physics-based prognostics algorithms with reviews. Reliab. Eng. Syst. Saf. 133, 223–236.
Arulampalam, M.S., Maskell, S., Gordon, N., Clapp, T., 2002. A tutorial on particle filters for online nonlinear/non-Gaussian Bayesian tracking. IEEE Trans. Signal Process. 50, 174–188.
Bouamama, B.O., Samantaray, A., Staroswiecki, M., Dauphin-Tanguy, G., 2003. Derivation of constraint relations from bond graph models for fault detection and isolation. Simulat. Series 35, 104–109.
Bressel, M., Hilairet, M., Hissel, D., Bouamama, B.O., 2016. Remaining useful life prediction and uncertainty quantification of proton exchange membrane fuel cell under variable load. IEEE Trans. Ind. Electron. 63, 2569–2577.
Bressel, M., Hilairet, M., Hissel, D., Ould Bouamama, B., 2016a. Extended kalman filter for prognostic of proton exchange membrane fuel cell. Appl. Energy 164, 220–227.
Bressel, M., Hilairet, M., Hissel, D., Ould Bouamama, B., 2016b. Remaining useful life prediction and uncertainty quantification of proton exchange membrane fuel cell under variable load. IEEE Trans. Ind. Electron.
J. Celaya, C. Kulkarni, G. Biswas, S. Saha, K. Goebel, A model-based prognostics methodology for electrolytic capacitors based on electrical overstress accelerated aging. (2011).
Chen, H., Pei, P., Song, M., 2015. Lifetime prediction and the economic lifetime of Proton Exchange Membrane fuel cells. Appl. Energy 142, 154–163.
Dai, J., Das, D., Ohadi, M., Pecht, M., 2013. Reliability risk mitigation of free air cooling through prognostics and health management. Appl. Energy 111, 104–112.
Daigle, M., Goebel, K., 2010. Model-based prognostics under limited sensing. In: 2010 IEEE Aerospace Conference, IEEE, pp. 1–12.
Daigle, M.J., Goebel, K., 2011. A model-Based prognostics approach applied to pneumatic valves. Int. J. Prognost. Health Manage. 2.
Daigle, M.J., Goebel, K., 2013. Model-based prognostics with concurrent damage progression processes. IEEE Trans. Syst. Man Cybern: Syst. 43, 535–546.
Daigle, M., Saha, B., Goebel, K., 2012. A comparison of filter-based approaches for model-based prognostics. In: 2012 IEEE Aerospace Conference, IEEE, pp. 1–10.
De Bruijn, F., Dam, V., Janssen, G., 2008. Review: durability and degradation issues of PEM fuel cell components. Fuel Cells 8, 3.
Djeziri, M.A., Merzouki, R., Bouamama, B.O., Dauphin-Tanguy, G., 2007. Robust fault diagnosis by using bond graph approach. IEEE/ASME Trans. Mechatron. 12, 599–611.
Djeziri, M.A., Ould Bouamama, B., Merzouki, R., 2009. Modelling and robust FDI of steam generator using uncertain bond graph model. J. Process Control 19, 149–162.
Djeziri, M.A., Bouamama, B.O., Dauphin-Tanguy, G., Merzouki, R., 2011. LFT bond graph model-Based robust fault detection and isolation. In: Bond Graph Modelling of Engineering Systems. Springer, pp. 105–133.
Doucet, A., Johansen, A.M., 2009. A Tutorial on Particle Filtering and Smoothing: Fifteen Years Later. Handbook of Nonlinear Filtering, 12., pp. 656–704.
Doucet, A., De Freitas, N., Gordon, N., 2001. An Introduction to Sequential Monte Carlo Methods. Springer.
Fowler, M.W., Mann, R.F., Amphlett, J.C., Peppley, B.A., Roberge, P.R., 2002. Incorporation of voltage degradation into a generalised steady state electrochemical model for a PEM fuel cell. J. Power Sources 106, 274–283.
Haykin, S., 2004. Kalman Filtering and Neural Networks, Vol. 47. John Wiley & Sons.
Hohenbichler, M., Gollwitzer, S., Kruse, W., Rackwitz, R., 1987. New light on first-and second-order reliability methods. Struct. Saf. 4, 267–284.
Hu, C., Jain, G., Tamirisa, P., Gorka, T., 2014. Method for estimating capacity and predicting remaining useful life of lithium-ion battery. Appl. Energy 126, 182–189.
Jardine, A.K., Lin, D., Banjevic, D., 2006. A review on machinery diagnostics and prognostics implementing condition-based maintenance. Mech. Syst. Sig. Process. 20, 1483–1510.
Jha, M., Dauphin-Tanguy, G., Ould Bouamama, B., 2014. Robust FDI based on LFT BG and relative activity at junction. In: 2014 European Control Conference (ECC), IEEE, pp. 938–943.
Jha, M.S., Dauphin-Tanguy, G., Ould-Bouamama, B., 2016. Particle filter based hybrid prognostics for health monitoring of uncertain systems in bond graph framework. Mech. Syst. Sig. Process. 75, 301–329.
Jouin, M., Gouriveau, R., Hissel, D., Péra, M.-C., Zerhouni, N., 2014a. Prognostics of PEM fuel cell in a particle filtering framework. Int. J. Hydrogen Energy 39, 481–494.
Jouin, M., Gouriveau, R., Hissel, D., Péra, M.-C., Zerhouni, N., 2014b. Prognostics of proton exchange membrane fuel cell stack in a particle filtering framework including characterization disturbances and voltage recovery. In: 2014 IEEE Conference on Prognostics and Health Management (PHM), IEEE, pp. 1–6.
Jouin, M., Gouriveau, R., Hissel, D., Péra, M.-C., Zerhouni, N., 2015. Joint particle filters prognostics for PEMFC power prediction at constant current solicitation. IEEE Trans. Reliab., 1–14.
Kundu, S., Fowler, M., Simon, L.C., Abouatallah, R., 2008. Reversible and irreversible degradation in fuel cells during open circuit voltage durability testing. J. Power Sources 182, 254–258.
Laffly, E., Péra, M.-C., Hissel, D., 2007. Polymer electrolyte membrane fuel cell modelling and parameters estimation for ageing consideration. IEEE Int. Sympos. Ind. Electr.
Larminie, J., Dicks, A., McDonald, M.S., 2003. Fuel Cell Systems Explained, Vol. 2. Wiley, New York.
Martínez, M.J., Shimpalee, S., Van Zee, J.W., 2008. Comparing predictions of PEM fuel cell behavior using Maxwell–Stefan and CFD approximation equations. Comput. Chem. Eng. 32, 2958–2965.
Mukherjee, A., Samantaray, A.K., 2006. Bond Graph in Modeling, Simulation and Fault Identification. IK International Pvt Ltd.
Ng, S.S., Xing, Y., Tsui, K.L., 2014. A naive Bayes model for robust remaining useful life prediction of lithium-ion battery. Appl. Energy 118, 114–123.
Oh, S.-D., Kim, K.-Y., Oh, S.-B., Kwak, H.-Y., 2012. Optimal operation of a 1-kW PEMFC-based CHP system for residential applications. Appl. Energy 95, 93–101.
Orchard, M.E., 2007. A Particle Filtering-based Framework for On-line Fault Diagnosis and Failure Prognosis. Georgia Institute of Technology.
Ould-Bouamama, B., El Harabi, R., Abdelkrim, M.N., Ben Gayed, M., 2012. Bond graphs for the diagnosis of chemical processes. Comput. Chem. Eng. 36, 301–324.
Ould-Bouamama, B., Chatti, N., Gehnin, A., 2013. Signed Bond Graph for health monitoring of PEM fuel cell. In: 5th International Conference of Development of Fuel Cells, Karlsruhe, Germany.
Park, J., Oh, H., Ha, T., Lee, Y.I., Min, K., 2015. A review of the gas diffusion layer in proton exchange membrane fuel cells: durability and degradation. Appl. Energy 155, 866–880.
Pei, P., Chen, H., 2014. Main factors affecting the lifetime of Proton Exchange Membrane fuel cells in vehicle applications: a review. Appl. Energy 125, 60–75.
Peraza, C., Diaz, J.G., Arteaga-Bravo, F.J., Villanueva, C., Gonzalez-Longatt, F., 2008. Modeling and simulation of PEM fuel cell with bond graph and 20sim. In: American Control Conference, 2008, IEEE, pp. 5104–5108.
Saha, B., Goebel, K., 2009. Modeling Li-ion battery capacity depletion in a particle filtering framework. Proceedings of the Annual Conference of the Prognostics and Health Management Society, 2909–2924.
Saha, B., Goebel, K., Christophersen, J., 2009a. Comparison of prognostic algorithms for estimating remaining useful life of batteries. Trans. Inst. Meas. Control.
Saha, B., Goebel, K., Poll, S., Christophersen, J., 2009b. Prognostics methods for battery health monitoring using a Bayesian framework. IEEE Trans. Instrum. Meas. 58, 291–296.
Saisset, R., Fontes, G., Turpin, C., Astier, S., 2006. Bond Graph model of a PEM fuel cell. J. Power Sources 156, 100–107.
Samantaray, A.K., Bouamama, B.O., 2008. Model-based Process Supervision: A Bond Graph Approach. Springer Science & Business Media.
Saxena, A., Celaya, J., Saha, B., Saha, S., Goebel, K., 2010. Metrics for offline evaluation of prognostic performance. Int. J. Prognost. Health Manage. 1, 4, color.
Schmittinger, W., Vahidi, A., 2008. A review of the main parameters influencing long-term performance and durability of PEM fuel cells. J. Power Sources 180, 1–14.
Schwabacher, M., 2005. A survey of data-driven prognostics. Proceedings of the AIAA Infotech@ Aerospace Conference, 1–5.
Sié Kam, C., Dauphin-Tanguy, G., 2005. Bond graph models of structured parameter uncertainties. J. Franklin Inst. 342, 379–399.
Sikorska, J., Hodkiewicz, M., Ma, L., 2011. Prognostic modelling options for remaining useful life estimation by industry. Mech. Syst. Signal Process. 25, 1803–1836.
Vachtsevanos, G., Lewis, F., Roemer, M., Hess, A., Wu, B., 2007. Intelligent Fault Diagnosis and Prognosis for Engineering Systems. John Wiley & Sons, Inc, New Jersey.
Venkatasubramanian, V., 2005. Prognostic and diagnostic monitoring of complex systems for product lifecycle management: challenges and opportunities. Comput. Chem. Eng. 29, 1253–1263.
Wang, Y., Chen, K.S., Mishler, J., Cho, S.C., Adroher, X.C., 2011. A review of polymer electrolyte membrane fuel cells: technology, applications: and needs on fundamental research. Appl. Energy 88, 981–1007.
Zhang, X., Hoo, K.A., 2011. Effective fault detection and isolation using bond graph-based domain decomposition. Comput. Chem. Eng. 35, 132–148.
Zio, E., Peloni, G., 2011. Particle filtering prognostic estimation of the remaining useful life of nonlinear components. Reliabi. Eng. Syst. Saf. 96, 403–409.
Ziogou, C., Voutetakis, S., Papadopoulou, S., Georgiadis, M.C., 2011. Modeling: simulation and experimental validation of a PEM fuel cell system. Comput. Chem. Eng. 35, 1886–1900.